Arabian Journal of Geosciences (2022) 15: 881
https://doi.org/10.1007/s12517-022-10160-z

ORIGINAL PAPER

Geochronology and geochemistry of Silurian pegmatites and related granodiorites from the Wudaogou area, southern East Kunlun Orogen, northern Qinghai–Tibetan Plateau

Jing Chen[1]

Received: 26 January 2022 / Accepted: 19 April 2022 / Published online: 29 April 2022

Abstract
Pegmatites (the Wudaogou pegmatite dikes) with minor beryllium mineralization have been discovered recently in the southern East Kunlun Orogen (EKO). This paper reports a study of zircon U–Pb dating, whole-rock geochemistry, and zircon Hf isotope and trace element compositions of the pegmatites and related granodiorite. Analyses of zircon morphology and in situ trace element compositions reveal that zircons from the pegmatite display spongeous texture in cathodoluminescence images, show extremely low Th/U ratios in the range of 0.002–0.013, and are enriched in heavy rare earth elements (REEs), with positive Ce and negative Eu anomalies. These features, as well as data patterns in a $(Sm/La)_N$-La diagram, suggest that zircons from the pegmatite formed during the transition stage between magmatic and hydrothermal zircons. The laser ablation–inductively coupled plasma–mass spectrometry zircon U–Pb age of the pegmatite is 425.8 ± 2.2 Ma (MSWD = 0.17), and that of the granodiorite is 427.7 ± 2.9 Ma (MSWD = 0.082), suggesting that the pegmatite formed simultaneously with or slightly later than the granodiorite. Both the pegmatite and granodiorite samples have high silica contents (SiO_2 = 72.31–76.10 wt.%), are peraluminous (A/CNK = 1.04–1.24), and belong to medium-K and shoshonitic series. The pegmatite samples have very low total REE contents (ΣREE = 5.39–8.08 ppm) with La_N/Yb_N ratios of 3.73–12.01 and strong positive Eu anomalies (Eu/Eu* = 1.47–2.75), whereas the granodiorite samples exhibit REE enrichment (ΣREE = 115.62–194.17 ppm) with $(La/Yb)_N$ = 9.35–35.53 and negative Eu anomalies (Eu/Eu* = 0.35–0.49). The REE contents of the pegmatite are markedly lower than those of the granodiorite, which may be related to the crystallization differentiation of accessory minerals, such as apatite, during magmatic evolution. Hf(t) values of the pegmatites range from − 3.89 to − 0.79 (mean = − 2.26), and those of the granodiorite range from − 7.53 to 2.73 (mean = − 2.48), which suggest a consistency of Hf(t) values of granodiorite and pegmatite. These geochemical characteristics imply that pegmatites and granites from the Wudaogou area have a genetic relationship and that the pegmatite being a more highly differentiated product of the same magma from which the granodiorite was formed. Both rock types formed in an extensional tectonic setting after the final closure of the Proto-Tethys Ocean in the EKO.

Keywords Pegmatites · Geochemistry · Zircon trace elements · Zircon U–Pb dating · Zircon Hf isotope · Wudaogou · East Kunlun Orogen

Introduction

Although volumetrically minor in the upper continental crust, pegmatites host abundant rare metal mineralization (e.g., Li, Be, Nb, and Ta) (London, 2018). Pegmatites and associated mineralization are generally thought to originate from extreme differentiation of a parent granite system, as they have granitic compositions and high fluxing components (Thomas et al. 2000; Barnes et al. 2012; London, 2018) or from formation by low degrees of partial melting of schists involving muscovite dehydration melting under

Communicated by Domenico M. Doronzo

✉ Jing Chen
2019194@qhnu.edu.cn

[1] School of Geographic Sciences, Qinghai Normal University, Xining 810000, China

amphibolite facies metamorphic conditions during compressional deformation of orogenic belts (Stewart, 1978; Henderson and Ihlen, 2004; Chen et al. 2020).

Pegmatites with minor beryllium mineralization (the Wudaogou Silurian pegmatites) have been discovered recently in the southern East Kunlun Orogen (EKO). A genetic model for these pegmatites has not yet been established, and the relationship between the pegmatites and co-existing granites remains unclear. In this paper, we present detailed field relationships, zircon U–Pb age, trace element, and Lu–Hf isotope data, and whole-rock major and trace element data for samples of pegmatites and host rock (granodiorite) from the Wudaogou area of the southern EKO. Results of the study allow us to (1) establish a genetic model for the Wudaogou pegmatites, (2) constrain the genetic links between the granitic pegmatites and associated granodiorites in this area, and (3) determine the tectonic environment of the magmatism that formed the pegmatites and granodiorites in the context of the closure of the Proto-Tethys Ocean in the EKO.

Geological setting and sample descriptions

The EKO is located south of the Qaidam Block and north of the Qiangtang-Songpan Block (Fig. 1a). The orogen is divided into three parts by the North Kunlun Fault and Central Kunlun Suture (Jiang et al. 1992); i.e., the North Kunlun Belt (NKB), Central Kunlun Belt (CKB), and South Kunlun Belt (SKB). Precambrian strata in the EKO have been highly metamorphosed and/or deformed, and they are dominated by the Paleoproterozoic Jinshuikou Group in the NKB and CKB (Li et al. 2008) and by the Mesoproterozoic–Neoproterozoic Kuhai and Wanbaogou groups in the SKB (Liu et al., 2016; Xu et al. 2016; Zhang et al. 2018; Wu et al. 2019). The EKO also contains abundant Permian–Triassic flysch successions and early Paleozoic and Middle–Late Triassic granitoid rocks (Liu et al. 2005; Wang et al. 2007, 2012; Chen et al. 2013).

The study area is located in the central SKB (Fig. 1b). The geology of the area comprises mainly Ordovician–Silurian Nachitai Group rocks, together with Silurian volcanic sedimentary formations and minor exposures of the Cambrian Shasongwula Formation and Triassic flysch successions (Fig. 1b). The Nachitai Group crops out in the study area and is composed predominantly of basaltic andesite, dacite, and rhyolite with island arc affinity, as well as pyroclastic rocks and turbidites interbedded with minor limestones (Dong et al. 2018).

The Wudaogou pegmatites are found in the north and east of the Wudaogou pluton in the Kunlunhe area of the SKB, where they intrude Silurian granitoids and the Nachitai Group (Fig. 1c). The dikes are gray white and sub-vertical, with widths of 0.2 to 9 m (Fig. 2a, b). The obtained sample (WDP) has pegmatitic grains measuring mainly 1–3 cm in length (and up to a maximum of 17 cm) and is composed mainly of microcline (40 vol.%), oligoclase (28 vol.%), quartz (24 vol.%), and muscovite (6 vol.%) (Fig. 2c), small amounts of garnet, tourmaline, apatite, and topaz, and trace amounts of beryl, chalcopyrite, tetrahedrite, and limonite.

The host rock of the pegmatite dikes is granodiorite (sample WDG), which consists of plagioclase (57 vol.%), K-feldspar (22 vol.%), quartz (16 vol.%), biotite (3 vol.%), and muscovite (1 vol.%), along with accessory minerals (1 vol.%) of zircon, rutile, and apatite. Plagioclase occurs as subhedral tabular grains (1–3 mm) displaying obvious sericitization. K-feldspar appears as grains generally 0.5–1.0 mm in size, has perthitic texture, and contains irregular cracks (Fig. 2d).

Analytical methods

Zircon U–Pb dating and Hf isotope and whole-rock geochemical analyses were carried out at Yanduzhongshi Geological Analysis Laboratories, Beijing, China. Zircons were handpicked, mounted in epoxy resin disks, and then polished until all mineral grains were approximately sectioned in half. Transmitted and reflected light and cathodoluminescence (CL) images were taken of the analyzed zircons to constrain their origins and to identify dating sites.

U–Pb dating and trace element analysis

Zircon U–Pb dating and trace element analyses were conducted simultaneously by laser ablation–inductively coupled plasma–mass spectrometry (LA-ICP-MS). Helium was used as a carrier gas and argon as a make-up gas. Each time-resolved analysis involved 20–30 s of blank signal and 40 s of sample signal acquisition. Offline data processing was conducted with ZSkits software, including selection of sample and blank signals, drift corrections, and calculation of elemental contents, U-Th-Pb isotope ratios, and ages. Isotopic fractionation correction was carried out by analysis of zircon standard 91,500. After 5–10 sample analyses, zircon 91,500 was analyzed twice along with one analysis of Plešovice zircon. Weighted mean ages were calculated and concordia diagrams plotted using Isoplot/Ex_ver3 software (Ludwig, 2003), and correction for common lead was made based on Andersen (2002). Ages obtained for zircon standards 91,500 and Plešovice are consistent with their recommended values (Wiedenbeck et al. 1995). Elemental compositions of the zircons were calibrated against multiple reference materials (BCR-2G and BIR-1G) and by internal standardization. The preferred values for element contents in the USGS reference glasses were taken from the GeoReM database (http://georem.mpch-mainz.gwdg.de/).

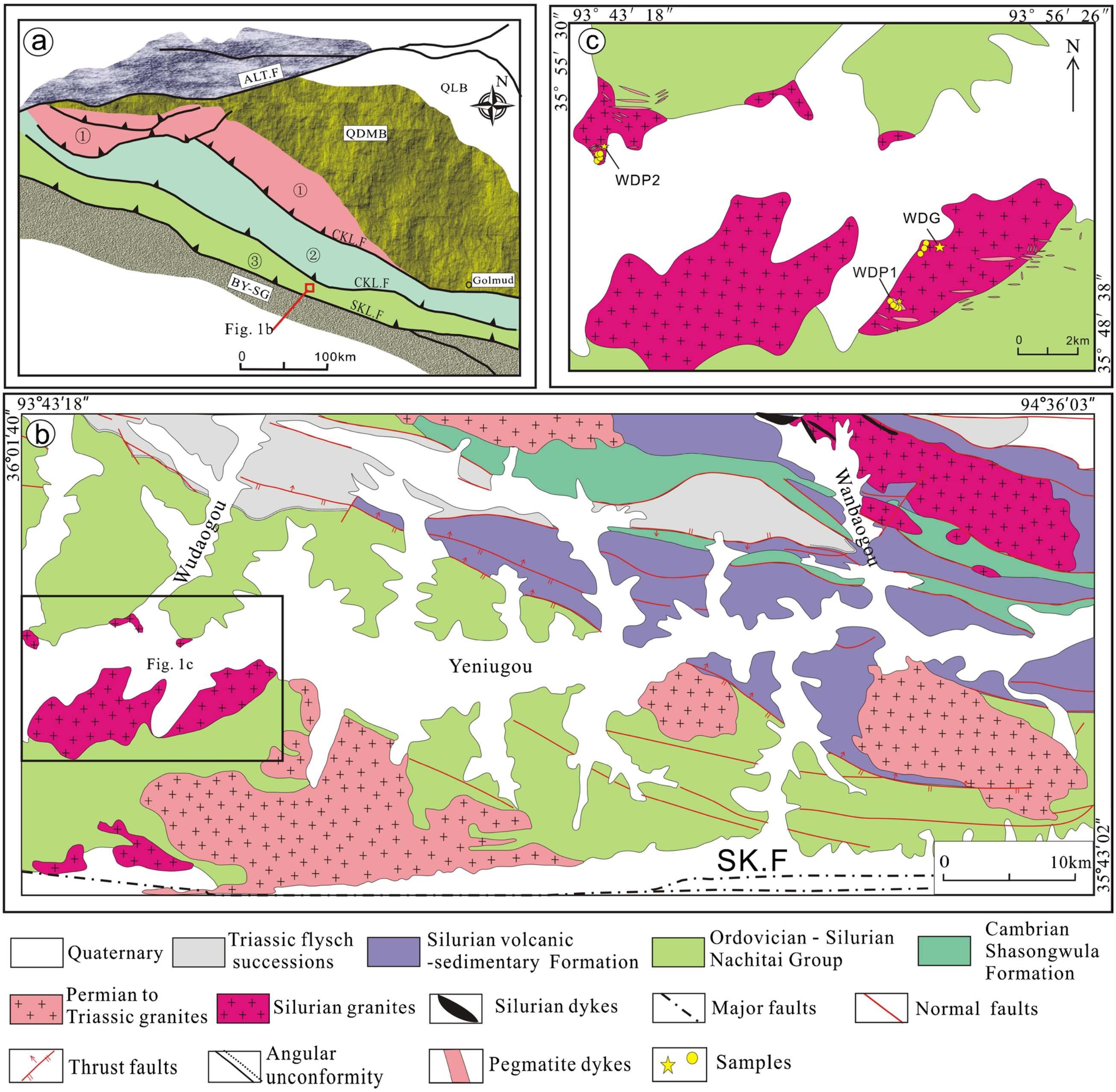

Fig. 1 Simplified geological map of part of **a** EKO, **b** Kunlun region, and **c** Wudaogou area. QT-SP, Qiangtang-Songpan Block; QDM.B, Qaidam Block; QLB, Qilian Block; ALT.F, Altun Tagh Fault; NKL.F, North Kunlun Fault; CKL.F, Central Kunlun Fault; SKL.F, South Kunlun Fault; ①, North Kunlun Belt; ②, Central Kunlun Belt; ③, South Kunlun Belt

Major and trace element analyses

Fresh whole-rock samples were broken into small pieces in a steel jaw crusher and then powdered to 200 mesh in an agate mill. H_2O^+, CO_2, and FeO contents were determined by gravimetric, volumetric, and titrimetric methods, respectively, and the other major elements were analyzed by X-ray fluorescence (XRF) spectrometry. Relative standard deviations (RSDs) for the major elements are < 1%. Trace elements were analyzed using an Agilent 7500a ICP-MS instrument. The sample preparation and digestion methods for ICP-MS analyses were the same as those described by Liu et al. (2008). The RSDs estimated from repeated analyses of three standard reference materials (G-2, AGV-1, and GSR-3) are < 5% for rare earth elements (REEs) and 5–12% for other elements. Detailed analytical procedures have been described by Qi et al. (2000).

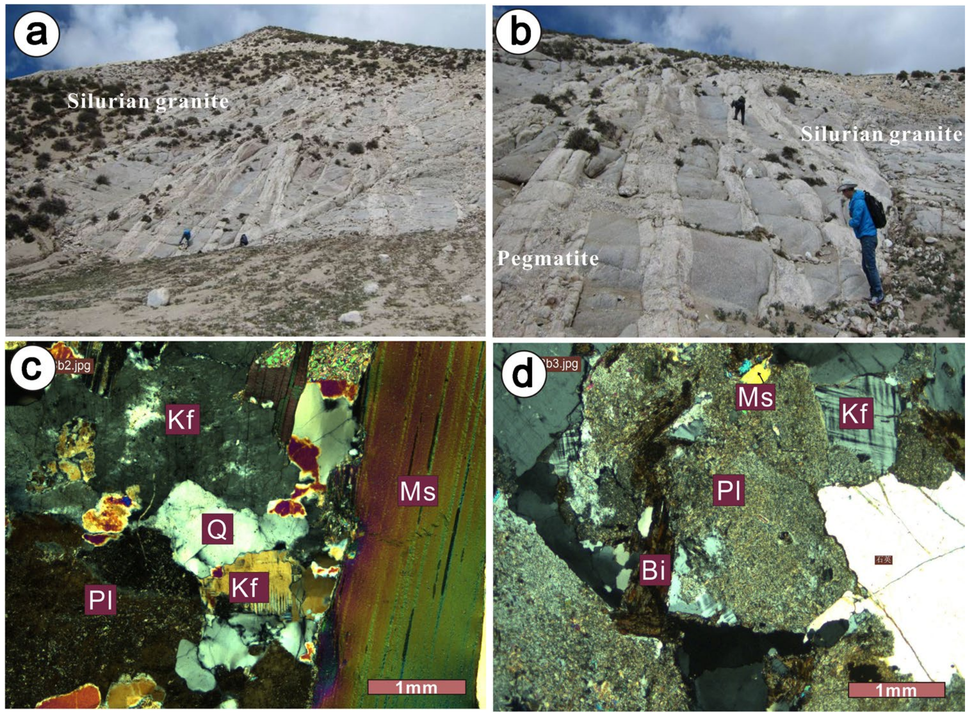

Fig. 2 **a** and **b** Wudaogou pegmatites; **c** thin section of Wudaogou pegmatite; and **d** Wudaogou granodiorite. Kf, K-feldspar; Pl, plagioclase; Q, quartz; Bi, biotite; Ms, muscovite

In situ Hf isotope analysis of zircon by LA-ICP-MS

Zircon Lu–Hf isotope analyses were carried out in situ using a NWR193 LA microprobe (Elemental Scientific Lasers) coupled to a Neptune multi-collector ICP-MS instrument. Instrumental conditions and data acquisition methods have been described by Wu et al. (2006). A stationary spot was used for the analyses, with a beam diameter of 40 µm. Helium was used as a carrier gas to transport the ablated sample from the LA cell to the ICP-MS torch via a mixing chamber where argon was introduced. To correct for isobaric interferences of ^{176}Lu and ^{176}Yb on ^{176}Hf, ^{176}Lu/^{175}Lu and ^{176}Yb/^{173}Yb ratios of 0.02658 and 0.796218, respectively, were used (e.g., Chu et al. 2002). The isotopic ratios of Yb were normalized to ^{172}Yb/^{173}Yb = 1.35274 (e.g., Chu et al. 2002) and Hf isotope ratios to ^{179}Hf/^{177}Hf = 0.7325 using an exponential law. The mass bias behavior of Lu was assumed to follow that of Yb; mass bias correction protocols have been described by Wu et al. (2006). Zircon standards 91,500 and Plešovice were used as reference standards during the period of analysis. Initial ^{176}Hf/^{177}Hf ratios and $\varepsilon_{Hf}(t)$ values were calculated with reference to the chondritic uniform reservoir (CHUR) of Blichert-Toft and Albarede (1997) at the time of zircon growth from the magma. Single-stage Hf model ages (T_{DM1}) were calculated relative to the depleted mantle with present-day ^{176}Hf/^{177}Hf = 0.28325 and ^{176}Lu/^{177}Hf = 0.0384 (e.g., Griffin et al. 2000).

Results

Zircon U–Pb dating and trace element data

Zircon grains from sample WDP are 100–300 µm long, irregular granular, opaque, and dark in color. CL images show that most zircons have spongeous texture and lack oscillatory zonation (Fig. 3). Zircons from the Wudaogou granodiorite are light brown to dark gray in color, subhedral–euhedral, and elongated to stubby in shape and have lengths of 90–250 µm with aspect ratios of 1:1–3:1. Oscillatory zonation is common in zircons, indicating a magmatic origin (Fig. 4b).

Zircons from the pegmatite contain contents of Th (5–27 ppm) and U (1685–3415 ppm) that yield Th/U ratios mostly between 0.002 and 0.013. In comparison, zircons from the granodiorite have Th contents of 1–392 ppm and U contents of 32–2971 ppm, with Th/U ratios of 0.01–2.25 (Table 1).

Zircon U–Pb data for the two samples from the study area yield weighted ^{206}Pb/^{238}U mean ages of 425.8 ± 2.2 Ma (MSWD = 0.17, n = 18) for the pegmatite and 427.7 ± 2.9 Ma (MSWD = 0.082, n = 12) for the granodiorite (Fig. 4a, b).

REE contents of zircons from the Wudaogou pegmatite are listed in Table 2. The total REE contents vary from 524 to 1301 ppm, with a mean of 820 ppm. Chondrite-normalized REE patterns (Fig. 5) exhibit marked depletion in light REEs (LREEs) and enrichment in heavy REEs (HREEs). Most of the zircons have positive Ce anomalies (Ce/Ce* = 1.11–8.20), except for two analysis points with

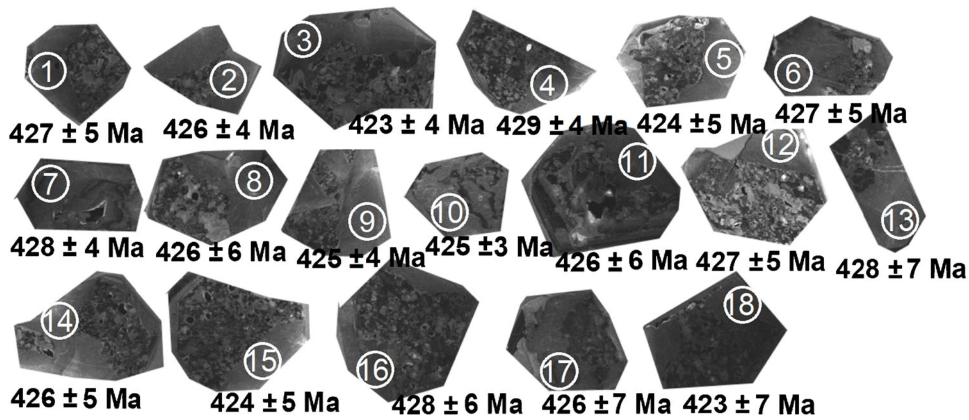

Fig. 3 Cathodoluminescence of Wudaogou pegmatite zircons (WDP sample)

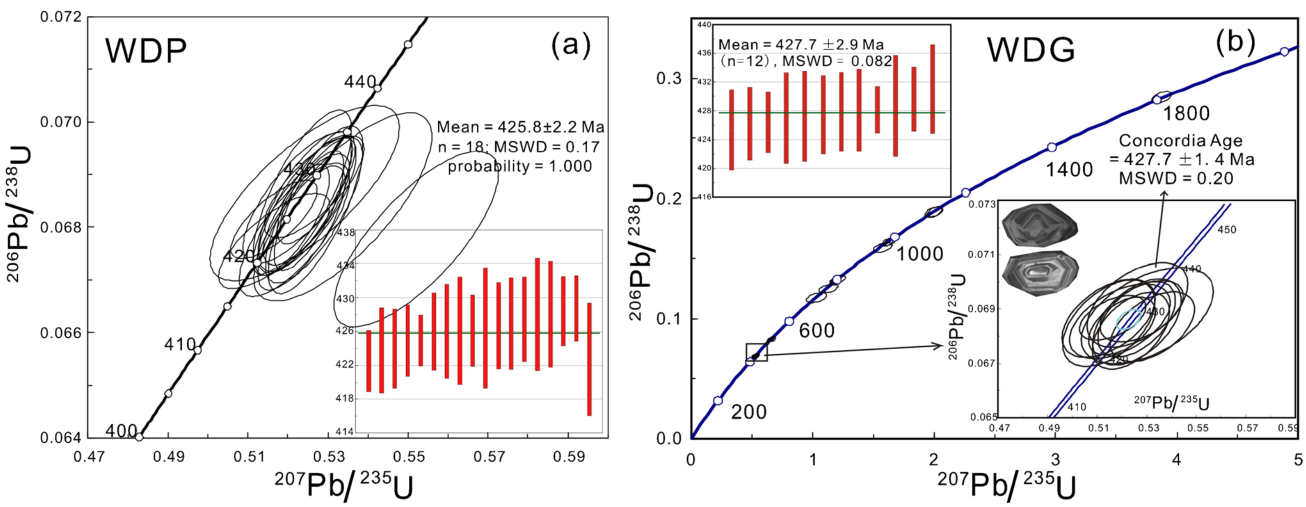

Fig. 4 Zircon concordia diagrams of the Wudaogou pegmatite and the related granodiorite

Ce/Ce* = 0.95 and 1.06, and moderate to large negative Eu anomalies (Eu/Eu* = 0.05–0.34), similar to those of typical magmatic zircons (Fig. 5) (Hoskin and Ireland, 2000; Hoskin, 2005). It is generally considered that negative Eu anomalies indicate zircon crystallization during plagioclase growth, as Eu^{2+} is preferentially incorporated into plagioclase (Hoskin, 2005). Strong enrichment in HREEs indicates that garnet growth did not occur during zircon crystallization (Sun et al. 2016).

Whole-rock major and trace element data

Results of major and trace element analyses are given in Table 3. All major element contents were normalized to a 100 wt.% on a volatile-free basis. The Wudaogou pegmatite samples (WDP-1, WDP-2, WDP-3, WDP-4) are characterized by high SiO_2 (73.61–76.10 wt.%), Al_2O_3 (13.73–16.06 wt.%), and $K_2O + Na_2O$ (8.38–9.72 wt.%) and low total Fe_2O_3 (0.58–0.63 wt.%), MgO (0.10–0.16 wt.%), and CaO (0.65–0.93 wt.%) contents. The Wudaogou granodiorite samples (WDG-1, WDG-2, WDG-3) have contents of SiO_2 = 72.31–75.65 wt.%, Al_2O_3 = 14.43–14.92 wt.%, $K_2O + Na_2O$ = 7.80–8.19 wt.%, total Fe_2O_3 = 1.19–2.18 wt.%, MgO = 0.31–0.62 wt.%, and CaO = 0.33–1.48 wt.%, similar to those of the pegmatites. Data for the WDP and WDG samples plot in the subalkaline series field in a total-alkali-silica (TAS) classification diagram (Fig. 6a) and belong to the medium-K and shoshonite series (Fig. 6b). The pegmatite and granodiorite have relatively high A/CNK values (1.04–1.24, mean = 1.14), suggesting that they have a peraluminous nature (Table 3).

The Wudaogou pegmatite samples (WDP-1 to WDP-4) have very low total REE contents, ranging from 5.39 to 8.08 ppm. The LREE/HREE and La_N/Yb_N ratios for the WDP samples are 2.81–6.35 and 3.73–12.01, respectively. The samples display positive Eu anomalies (Eu/Eu* = 1.47–2.75) (Fig. 7a). In N-MORB-normalized diagrams (Fig. 7b), the WDP samples are enriched in Rb, U, Sr, P, and Hf and depleted in Th, Nd, Zr, and Ti. Chondrite-normalized REE patterns of the Wudaogou

Table 1 LA-ICP-MS zircon U–Pb analyses for the Wudaogou pegmatite and the related granite (WDP and WDG) from the SKB

Sample	Contents (ppm) and ratios			Isotope ratios and errors						Ages and errors			
WDP	U	Th	Th/U	^{207}Pb/^{206}Pb	1σ	^{207}Pb/^{235}U	1σ	^{206}Pb/^{238}U	1σ	^{206}Pb/^{238}U	1σ	^{207}Pb/^{235}U	1σ
1	2414	9	0.004	0.05560	0.00075	0.52417	0.00775	0.06847	0.00089	427	5	428	5
2	2227	11	0.005	0.05558	0.00073	0.52458	0.00712	0.06833	0.00069	426	4	428	5
3	2455	21	0.009	0.05536	0.00114	0.51661	0.00918	0.06774	0.00059	423	4	423	6
4	2368	9	0.004	0.05537	0.00063	0.52657	0.00821	0.06876	0.00064	429	4	430	5
5	1885	8	0.004	0.05570	0.00082	0.52343	0.00720	0.06798	0.00078	424	5	427	5
6	2767	11	0.004	0.05509	0.00066	0.52278	0.00923	0.06856	0.00082	427	5	427	6
7	1685	6	0.004	0.05547	0.00042	0.52676	0.00622	0.06871	0.00068	428	4	430	4
8	2984	16	0.006	0.05568	0.00046	0.52648	0.00800	0.06832	0.00092	426	6	429	5
9	1832	8	0.004	0.05539	0.00088	0.52085	0.00628	0.06814	0.00069	425	4	426	4
10	1806	23	0.013	0.05478	0.00085	0.51652	0.00713	0.06814	0.00049	425	3	423	5
11	1995	14	0.007	0.05595	0.00059	0.52690	0.00779	0.06833	0.00105	426	6	430	5
12	2081	8	0.004	0.05542	0.00083	0.52490	0.00805	0.06843	0.00084	427	5	428	5
13	2123	9	0.004	0.05557	0.00171	0.52419	0.01560	0.06865	0.00110	428	7	428	10
14	2734	13	0.005	0.05560	0.00046	0.52529	0.00576	0.06832	0.00075	426	5	429	4
15	1771	9	0.005	0.05539	0.00103	0.52164	0.00910	0.06795	0.00083	424	5	426	6
16	3328	22	0.007	0.05534	0.00062	0.52360	0.00813	0.06866	0.00103	428	6	428	5
17	2426	5	0.002	0.05652	0.00193	0.53370	0.01468	0.06838	0.00118	426	7	434	10
18	3415	27	0.008	0.05920	0.00140	0.55206	0.01358	0.06777	0.00110	423	7	446	9
WDG													
1	926	44	0.050	0.05545	0.00140	0.53392	0.01515	0.06947	0.00093	433	6	434	10
2	297	99	0.330	0.05673	0.00091	0.62329	0.01138	0.07957	0.00083	494	5	492	7
3	152	132	0.870	0.07678	0.00128	2.00032	0.04883	0.18857	0.00287	1114	16	1116	17
4	1819	21	0.010	0.05533	0.00102	0.52630	0.01341	0.06915	0.00102	431	6	429	9
5	143	206	1.440	0.06332	0.00258	1.02843	0.05542	0.11721	0.00274	714	16	718	28
6	520	42	0.080	0.05551	0.00098	0.52601	0.01174	0.06852	0.00104	427	6	429	8
7	783	72	0.090	0.07403	0.00188	0.94450	0.02914	0.09275	0.00140	572	8	675	15
8	359	144	0.400	0.07198	0.00160	1.57924	0.05140	0.15923	0.00268	953	15	962	20
9	659	224	0.340	0.05434	0.00085	0.51473	0.01222	0.06848	0.00105	427	6	422	8
10	382	45	0.120	0.05565	0.00106	0.52591	0.01027	0.06862	0.00091	428	6	429	7
11	156	53	0.340	0.05449	0.00118	0.51464	0.01234	0.06866	0.00094	428	6	422	8
12	436	269	0.620	0.05628	0.00167	0.53031	0.01760	0.06876	0.00116	429	7	432	12
13	406	43	0.100	0.05471	0.00102	0.51915	0.01335	0.06855	0.00090	427	5	425	9
14	326	154	0.470	0.05657	0.00105	0.53233	0.01122	0.06835	0.00084	426	5	433	7
15	133	78	0.590	0.07725	0.00122	2.00307	0.03868	0.18872	0.00271	1114	15	1117	13
16	246	18	0.070	0.05557	0.00108	0.52794	0.01104	0.06892	0.00074	430	4	430	7
17	215	69	0.320	0.05788	0.00113	0.65720	0.01378	0.08263	0.00091	512	5	513	8
18	40	18	0.450	0.06657	0.00228	1.20727	0.04386	0.13245	0.00203	802	12	804	20
19	485	165	0.340	0.07204	0.00072	1.61940	0.02653	0.16349	0.00213	976	12	978	10
20	295	28	0.100	0.05463	0.00093	0.51628	0.00878	0.06868	0.00054	428	3	423	6
21	167	1	0.010	0.12770	0.00135	6.05315	0.08921	0.34391	0.00380	1905	18	1984	13
22	103	47	0.450	0.06619	0.00150	1.18329	0.02919	0.13009	0.00172	788	10	793	14
23	179	76	0.420	0.05769	0.00170	0.65847	0.02238	0.08267	0.00133	512	8	514	14
24	497	99	0.200	0.05505	0.00070	0.52001	0.00886	0.06838	0.00070	426	4	425	6
25	165	73	0.440	0.09884	0.00087	3.87089	0.05231	0.28406	0.00325	1612	16	1608	11
26	237	153	0.640	0.07251	0.00108	1.63551	0.03033	0.16393	0.00216	979	12	984	12
27	2971	392	0.130	0.05556	0.00073	0.52360	0.01022	0.06820	0.00093	425	6	428	7
28	32	73	2.250	0.06620	0.00292	1.12719	0.05146	0.12485	0.00240	758	14	766	25

Table 2 Rare earth elements concentrations (ppm) of zircons from the Wudaogou pegmatite

WDP	La	Ce	Pr	Nd	Sm	Eu	Gd	Tb	Dy	Ho	Er	Tm	Yb	Lu	ΣREE	LREE	HREE	δEu	δCe
1	0.106	0.627	0.128	0.276	0.473	0.123	2.86	2.67	46	21	129	39	467	87	796	1.73	795	0.25	1.14
2	0.019	0.149	0.021	0.159	0.152	0.047	2.75	2.37	47	23	139	43	513	98	868	0.55	867	0.11	1.58
3	0.120	0.798	0.084	0.460	1.260	0.168	5.69	3.54	57	25	144	41	451	86	815	2.89	812	0.16	1.87
4	0.024	0.163	0.026	0.062	0.300	0.025	2.77	2.26	48	25	155	48	579	111	972	0.60	972	0.06	1.44
5	0.021	0.055	0.000	0.050	0.172	0.045	1.96	1.77	36	17	103	31	356	65	611	0.34	611	0.14	0.95
6	0.050	0.176	0.031	0.238	0.165	0.062	2.59	2.21	48	23	148	47	574	112	957	0.72	956	0.16	1.06
7	0.038	0.125	0.009	0.047	0.289	0.046	2.12	1.93	34	15	87	26	303	54	524	0.56	523	0.13	1.58
8	0.734	1.682	0.140	0.494	2.131	0.303	13.41	6.63	90	34	175	50	572	109	1056	5.48	1051	0.13	1.20
9	0.025	0.074	0.009	0.015	0.130	0.018	2.32	1.91	39	18	107	33	364	66	631	0.27	631	0.05	1.18
10	0.012	0.259	0.005	0.107	0.275	0.072	2.32	2.04	39	18	102	30	333	61	588	0.73	587	0.19	8.20
11	0.042	0.549	0.027	0.217	0.371	0.117	2.13	2.00	40	19	111	34	402	72	684	1.32	683	0.31	3.88
12	0.025	0.109	0.000	0.053	0.189	0.109	3.13	2.72	49	20	103	27	280	45	531	0.49	531	0.23	1.44
13	0.035	0.329	0.053	0.075	0.688	0.170	4.48	3.26	52	21	121	37	451	91	782	1.35	781	0.22	1.51
14	0.014	0.296	0.020	0.074	0.240	0.136	3.34	3.10	62	29	173	51	584	107	1013	0.78	1012	0.26	3.58
15	0.034	0.411	0.040	0.158	0.256	0.154	2.85	2.42	42	19	108	32	348	63	618	1.05	617	0.34	2.39
16	0.124	0.679	0.059	0.554	0.871	0.275	7.42	4.79	77	34	187	54	610	112	1089	2.56	1087	0.23	1.93
17	0.069	0.693	0.028	0.169	0.442	0.056	3.24	2.32	42	18	118	41	550	113	889	1.46	888	0.10	3.84
18	0.163	1.053	0.139	1.394	1.425	0.327	7.28	4.33	77	36	212	63	750	146	1301	4.50	1296	0.25	1.60

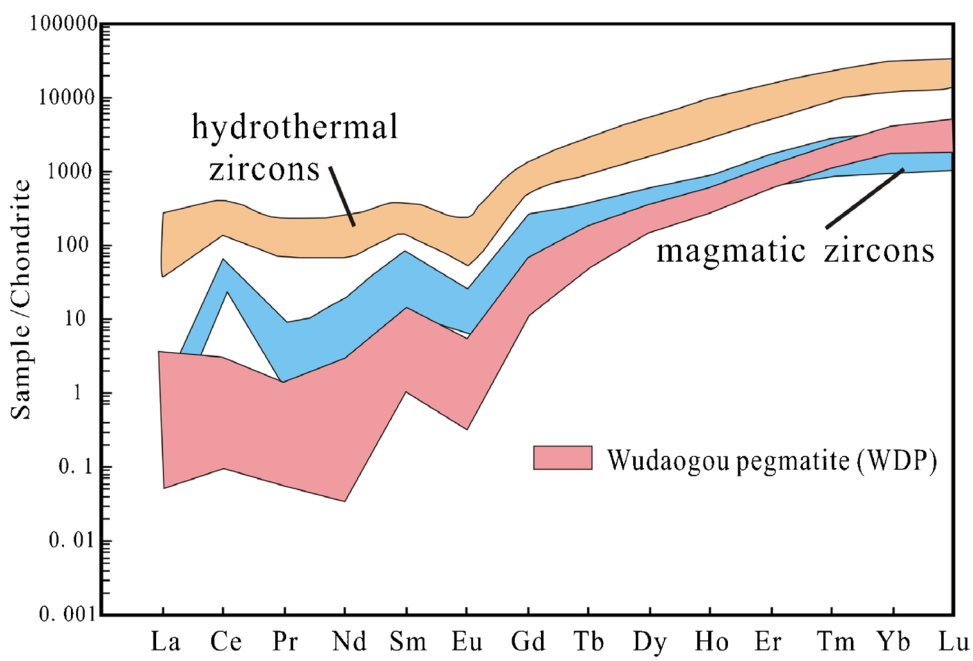

Fig. 5 Chondrite-normalized REE patterns of zircons of the Wudaogou pegmatite (normalization values after Sun and McDonough (1989)). Typical magmatic zircon and hydrothermal zircon data are after Hoskin and Ireland (2000) and Hoskin (2005)

granodiorite samples (WDG-1 to WDG-3) show REE enrichment (ΣREE = 115.62–194.17 ppm) and pronounced LREE enrichment (LREE/HREE = 7.50–17.11), with $(La/Yb)_N$ = 9.35–35.53. These samples exhibit negative Eu anomalies (Eu/Eu* = 0.35–0.49) and are enriched in Rb, Th, U, Nd, Zr, and Hf and depleted in Nb, Sr, P, and Ti. Negative P, Sr, and Ti anomalies may indicate fractional crystallization of apatite, plagioclase, and Ti-bearing phases (e.g., rutile, ilmenite, and titanite), respectively.

Zircon in situ Hf isotope data

In situ zircon Lu–Hf analyses undertaken during this study used the same analysis spots as used for zircon U–Pb dating, with results for both two samples given in Table 4. Zircons from the Wudaogou pegmatite yield a narrow range of initial $^{176}Hf/^{177}Hf$ (0.282407–0.282489) values, with calculated εHf(t) values from − 3.89 to − 0.79 (Fig. 8a, b) (mean of − 2.26) and T_{DM2} ages of 1664–1465 Ma.

Table 3 Composition of major (wt%) and trace elements (ppm) of the Wudaogou pegmatite (WDP) and granodiorite (WDG)

Sample	WDP-1	WDP-2	WDP-3	WDP-4	WDG-1	WDG-2	WDG-3
Lithology	Pegmatite				Granodiorite		
SiO_2	72.80	75.92	75.46	74.06	70.90	75.07	71.39
TiO_2	0.01	0.01	0.00	0.00	0.27	0.14	0.28
Al_2O_3	15.88	13.70	14.24	14.45	14.63	14.32	14.52
TFe_2O_3	0.62	0.62	0.58	0.59	2.14	1.18	2.13
MnO	0.03	0.03	0.03	0.03	0.03	0.04	0.04
MgO	0.14	0.16	0.10	0.14	0.61	0.31	0.59
CaO	0.92	0.76	0.65	0.77	1.35	0.33	1.45
Na_2O	5.18	3.39	3.91	3.47	3.43	4.48	3.26
K_2O	3.19	4.97	4.62	6.24	4.60	3.28	4.40
P_2O_5	0.13	0.20	0.20	0.15	0.09	0.08	0.10
LOS	1.04	0.60	0.67	0.60	1.75	0.81	1.81
Total	99.94	100.35	100.46	100.50	99.78	100.04	99.96
A/NK	1.33	1.25	1.25	1.16	1.38	1.31	1.43
A/CNK	1.16	1.11	1.13	1.04	1.12	1.24	1.14
La	1.92	1.30	1.88	1.34	47.56	24.92	45.26
Ce	3.19	2.23	2.89	2.03	87.08	49.76	82.34
Pr	0.33	0.23	0.32	0.21	9.20	5.12	8.90
Nd	1.10	0.83	1.02	0.68	32.46	18.01	31.19
Sm	0.31	0.29	0.28	0.21	6.49	3.68	6.34
Eu	0.13	0.15	0.13	0.16	0.65	0.53	0.62
Gd	0.21	0.24	0.19	0.13	3.92	2.71	3.86
Tb	0.07	0.10	0.07	0.05	0.72	0.66	0.73
Dy	0.40	0.67	0.42	0.29	2.98	4.28	3.16
Ho	0.07	0.12	0.07	0.05	0.49	0.93	0.53
Er	0.17	0.33	0.21	0.13	1.35	2.52	1.38
Tm	0.02	0.05	0.03	0.02	0.15	0.32	0.16
Yb	0.14	0.25	0.20	0.08	0.96	1.91	1.03
Lu	0.02	0.03	0.03	0.01	0.15	0.26	0.16
Rb	126.23	180.70	189.90	193.29	146.86	98.31	140.65
Ba	81.12	116.25	108.93	169.52	775.89	523.99	752.37
Ta	3.41	2.33	1.69	1.63	0.89	0.57	0.94
Nb	6.45	4.56	5.36	2.04	6.78	3.99	7.04
Hf	0.22	0.09	0.21	0.20	5.46	3.44	5.36
Zr	2.36	0.83	2.31	2.40	143.90	87.40	142.03
Y	2.25	3.84	2.37	1.63	14.70	27.13	15.61
Ga	20.33	14.01	16.85	11.59	19.15	16.36	19.41
Sr	42.21	43.70	35.51	58.03	164.57	136.35	148.48
Th	0.72	0.52	0.47	0.57	16.97	10.64	16.24
Pb	23.83	37.14	28.24	47.63	25.82	22.88	25.75
U	0.29	0.48	0.38	0.83	8.08	2.41	11.60
Cs	7.80	7.70	9.45	7.95	5.79	3.46	5.45
Sc	1.26	0.83	0.95	0.29	6.28	3.98	6.48
Li	7.09	5.87	5.39	8.82	34.05	23.65	35.05
Be	10.08	5.10	5.26	5.23	4.82	4.17	4.89
Ti	135.50	126.78	102.35	82.68	1475.63	820.95	1489.16
ΣREE	8.08	6.82	7.74	5.39	194.17	115.62	185.65
LREE	6.98	5.03	6.52	4.63	183.45	102.02	174.65
HREE	1.10	1.79	1.22	0.76	10.72	13.60	11.00
LREE/HREE	6.35	2.81	5.34	6.09	17.11	7.50	15.88
La_N/Yb_N	9.84	3.73	6.74	12.01	35.53	9.35	31.64
δEu	1.47	1.69	1.63	2.75	0.37	0.49	0.35
δCe	0.90	0.92	0.84	0.84	0.96	1.02	0.95

LOI, loss on ignition; *A/CNK*, molecular $Al_2O_3/(CaO+Na_2O+K_2O)$; *A/NK*, molecular $Al_2O_3/(Na_2O+K_2O)$; Eu/Eu*is a measure of the europium anomaly when compared to Sm and Gd. $Eu/Eu^* = Eu_N/(Sm_N \times Gd_N)^{0.5}$. Relative standard deviations (RSDs) for the major elements are < 1%. RSDs estimated from repeated analyses of three standard reference materials (G-2, AGV-1, and GSR-3) are < 5% for rare earth elements (REEs) and 5–12% for other elements

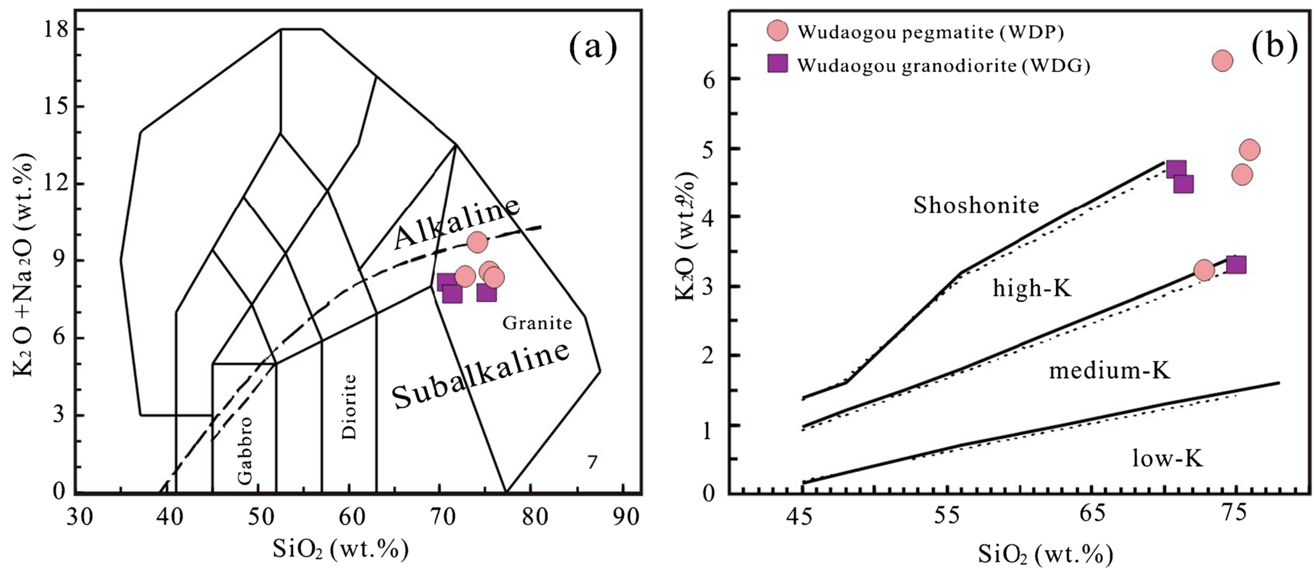

Fig. 6 **a** Total alkali-silica diagram (after Wilson (1989)). **b** SiO_2 versusK_2O for the studied rocks (continuous line is after Peccerillo and Taylor (1976); dotted line is after Middlemost (1985))

Zircons from the Wudaogou granodiorite have uniform initial $^{176}Hf/^{177}Hf$ ratios (0.282299–0.282594) and calculated εHf(t) values that range from − 7.53 to 2.73 (Fig. 8a, b) (mean of − 2.48). Their T_{DM2} ages range from 1897 to 1242 Ma and are indicative of crustal contamination by Paleoproterozoic–Mesoproterozoic rocks. The Wudaogou pegmatite and granodiorite samples of the present study and four granitic samples from Chen et al. (2021b) have similar εHf(t) values (Fig. 8a), which suggests that they were probably derived from the same source.

Discussion

Genesis of zircons from the Wudaogou pegmatite

The studied pegmatite sample has high zircon U contents (mostly > 2000 ppm). High-U zircons may yield a higher-than-expected U–Pb apparent age (the "high-U effect") and can also be influenced by the radioactive Pb loss effect yielding a lower-than-expected apparent age (Li and Chou, 2016). Therefore, it can be difficult to reliably determine the age of high-U zircon. However, in the present study, $^{206}Pb/^{238}U$ ages of analytical spots of pegmatite sample do

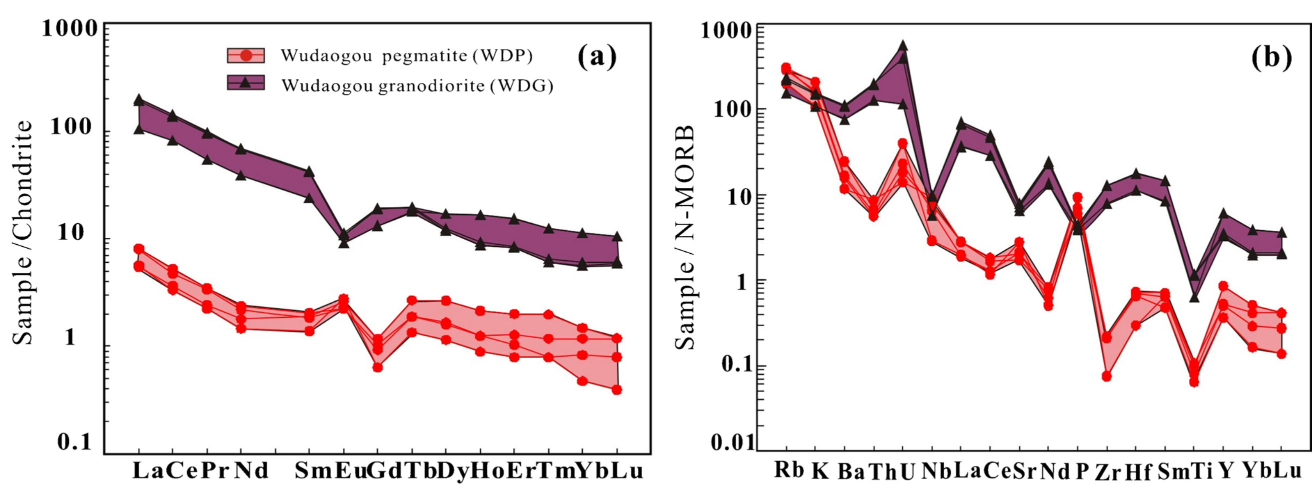

Fig. 7 Chondrite-normalized REE pattern (**a**) and primitive mantle-normalized spider diagrams (**b**) from pegmatites of Wudaogou area

Table 4 Zircon in situ Hf isotope composition of the pegmatites

Samples	t (Ma)	$^{176}Yb/^{177}Hf$	$^{176}Lu/^{177}Hf$	±2σ	$^{176}Hf/^{177}Hf$	±2σ	$\varepsilon_{Hf}(t)$	2 s	T_{DM1} (Ga)	2 s	T_{DMC} (Ga)	2 s	$f_{Lu/Hf}$
WDG-01	433	0.049445	0.001170	0.000020	0.282299	0.000022	−7.53	0.78	1351	31	1897	48	−0.96
WDG-04	431	0.082557	0.001943	0.000041	0.282579	0.000023	2.10	0.83	977	34	1286	52	−0.94
WDG-06	427	0.071116	0.001479	0.000080	0.282593	0.000024	2.66	0.86	945	35	1248	54	−0.96
WDG-09	427	0.023878	0.000524	0.000009	0.282411	0.000023	−3.53	0.81	1174	32	1640	51	−0.98
WDG-10	428	0.050736	0.001301	0.000046	0.282516	0.000034	0.01	1.20	1049	48	1417	76	−0.96
WDG-11	428	0.034165	0.000749	0.000024	0.282345	0.000019	−5.89	0.69	1272	27	1790	43	−0.98
WDG-12	429	0.035222	0.000832	0.000013	0.282377	0.000021	−4.77	0.74	1231	29	1720	46	−0.97
WDG-13	427	0.050294	0.001170	0.000024	0.282447	0.000024	−2.43	0.85	1143	34	1571	54	−0.96
WDG-14	426	0.051685	0.001270	0.000018	0.282594	0.000023	2.73	0.83	938	33	1242	52	−0.96
WDG-20	428	0.020589	0.000462	0.000002	0.282347	0.000019	−5.73	0.66	1259	26	1780	41	−0.99
WDG-24	426	0.012033	0.000284	0.000019	0.282417	0.000018	−3.26	0.64	1158	25	1622	40	−0.99
WDG-27	425	0.054535	0.001083	0.000009	0.282401	0.000021	−4.06	0.73	1204	29	1672	46	−0.97
WDP-01	427	0.024968	0.000676	0.000016	0.282465	0.000011	−1.65	0.39	1103	15	1521	24	−0.98
WDP-02	426	0.044800	0.001192	0.000047	0.282419	0.000014	−3.45	0.50	1183	20	1634	31	−0.96
WDP-03	423	0.022815	0.000671	0.000016	0.282426	0.000018	−3.13	0.64	1157	25	1611	40	−0.98
WDP-04	429	0.031839	0.000842	0.000032	0.282438	0.000012	−2.62	0.42	1146	17	1584	27	−0.97
WDP-05	424	0.013167	0.000312	0.000007	0.282442	0.000011	−2.43	0.39	1124	15	1568	24	−0.99
WDP-06	427	0.025147	0.000634	0.000011	0.282440	0.000012	−2.52	0.42	1137	17	1576	27	−0.98
WDP-07	428	0.056053	0.001444	0.000040	0.282407	0.000014	−3.89	0.50	1208	20	1664	31	−0.96
WDP-08	426	0.020508	0.000490	0.000007	0.282451	0.000011	−2.12	0.39	1117	15	1550	24	−0.99
WDP-09	425	0.024560	0.000630	0.000007	0.282443	0.000012	−2.46	0.42	1132	17	1571	27	−0.98
WDP-10	425	0.018854	0.000462	0.000007	0.282489	0.000013	−0.79	0.46	1064	18	1465	29	−0.99
WDP-11	426	0.011084	0.000237	0.000011	0.282455	0.000009	−1.90	0.32	1104	12	1537	20	−0.99
WDP-12	427	0.042855	0.001130	0.000030	0.282486	0.000013	−1.04	0.46	1087	18	1483	29	−0.97
WDP-13	428	0.007364	0.000154	0.000001	0.282439	0.000011	−2.40	0.39	1124	15	1570	24	−1.00
WDP-14	426	0.024506	0.000522	0.000045	0.282467	0.000014	−1.56	0.50	1096	19	1515	31	−0.98
WDP-15	424	0.026418	0.000614	0.000006	0.282459	0.000013	−1.92	0.46	1110	18	1536	29	−0.98

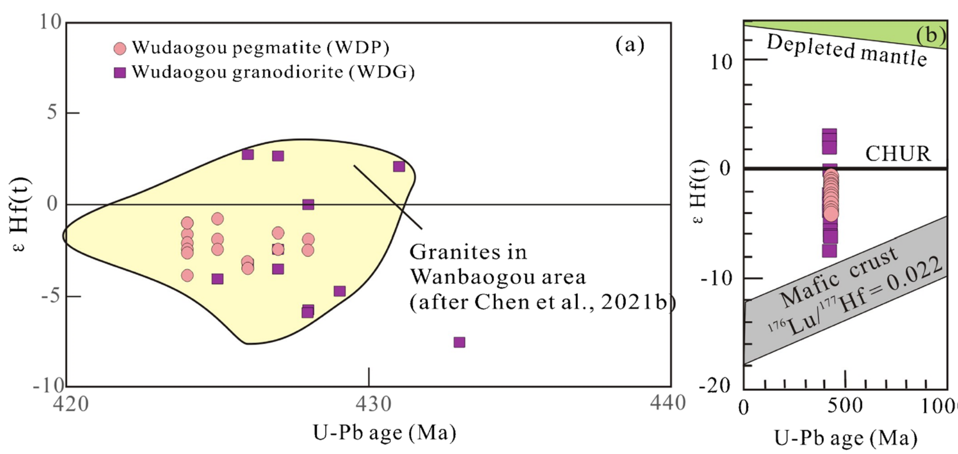

Fig. 8 Plot showing variations in Hf(t) values and inferred crystallization ages for the magmatic zircons analyzed during this study. CHUR, chondritic uniform reservoir. The $^{176}Lu/^{177}Hf$ values of the mafic lower crust and the average continental crust are from Kemp et al. (2006)

not show systematic variation with respect to U contents (Fig. 9a). Therefore, the possible influence of high U on the determined zircon U–Pb ages of the studied pegmatite can be disregarded.

Chondrite-normalized REE patterns of the Wudaogou pegmatite samples, which show positive Ce anomalies (Ce/Ce* = 0.95–8.20) and negative Eu anomalies (Eu/Eu* = 0.05–0.34) (Fig. 5), exhibit characteristics of magmatic zircons, whereas features observed in CL images and the very low Th/U ratios (Th/U = 0. 002–0. 0133) differ from those of magmatic zircons (Hoskin and Black, 2000). The origin of zircons can also be determined by a $(Sm/La)_N$-La diagram (Hoskin, 2005). According to Fig. 9b, all analysis points of Wudaogou pegmatite zircons fall in the transition region between magmatic zircons and hydrothermal zircons, indicating that the zircons were formed into the transition stage between magmatic zircons and hydrothermal zircons.

Genetic model for the Wudaogou pegmatite

The Wudaogou pegmatites occur as dike swarms sharply bounded by granodiorite (Fig. 2a, b) and the Nachitai Group (Fig. 1c) and are confined to a region within 1–1.5 km of the inner or outer contact zone between the dikes and host rocks.

The LA-ICP-MS zircon U–Pb ages of the Wudaogou pegmatite and granodiorite are 425.8 ± 2.2 Ma and 427.7 ± 2.9 Ma, respectively, suggesting that the pegmatite formed at the simultaneously time as or slightly later than the granodiorite and that the pegmatite dikes represent further magmatic evolution relative to the granodiorite by extreme differentiation (e.g., Hulsbosch et al. 2014; London, 2018).

In terms of geochemistry, the Wudaogou pegmatite and granodiorite are similar in composition, with characteristics of high silica, enrichment in alkalis, and peraluminosity. REE contents of the pegmatite are much lower than those of the granodiorite, suggesting crystallization differentiation of accessory minerals, such as apatite, during magmatic evolution. The distribution coefficients of these accessory minerals in the residual melt were high, which would have influenced the contents of REE elements (Fujimaki, 1986; Mahood and Hildreth, 1983; Yurimoto et al. 1990). Figure 10 shows that the variation in REE content of the pegmatite may have been caused by crystal fractionation of apatite and allanite.

Zircon Hf isotopes can be reliably used for inferring geological evolution and for tracing magmatic rock source (Wu et al. 2007). εHf(t) values of the studied Wudaogou pegmatite show a narrow range of negative values ranging from − 3.89 to − 0.79 (Fig. 8a, b) (mean of − 2.26). The negative εHf(t) values indicate that the magmatic source of the pegmatite dikes comprised melted crustal materials (Hawkesworth and Kemp, 2006), and the narrow range of values suggests that the magmatic source region was simple. εHf(t) values of the Wudaogou granodiorite range more widely from − 7.53 to 2.73 (Fig. 8a, b) (mean of − 2.48).

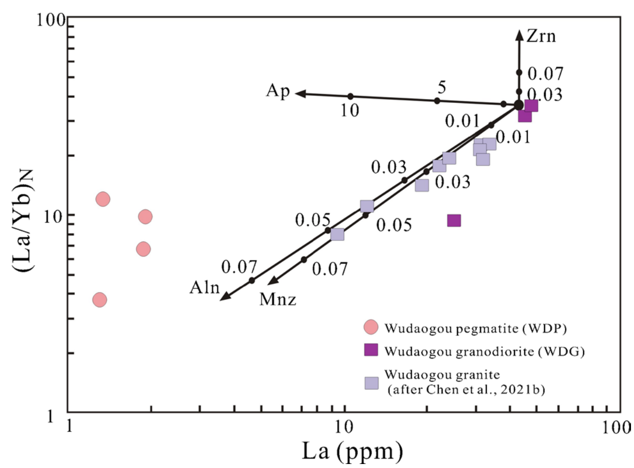

Fig. 10 (La /Yb) $_N$ vs. La plot of the Wudaogou pegmatites. Apatite distribution coefficient is after Fujimaki (1986); zircon and allanite distribution coefficient is after Mahood and Hildreth (1983); distribution coefficient of monazite is after Yurimoto et al. (1990). Pl, plagioclase; Kf, potassium feldspar; Bt, biotite; Aln, allanite; Mnz, monazite; Ap, apatite; and Zrn, zircon

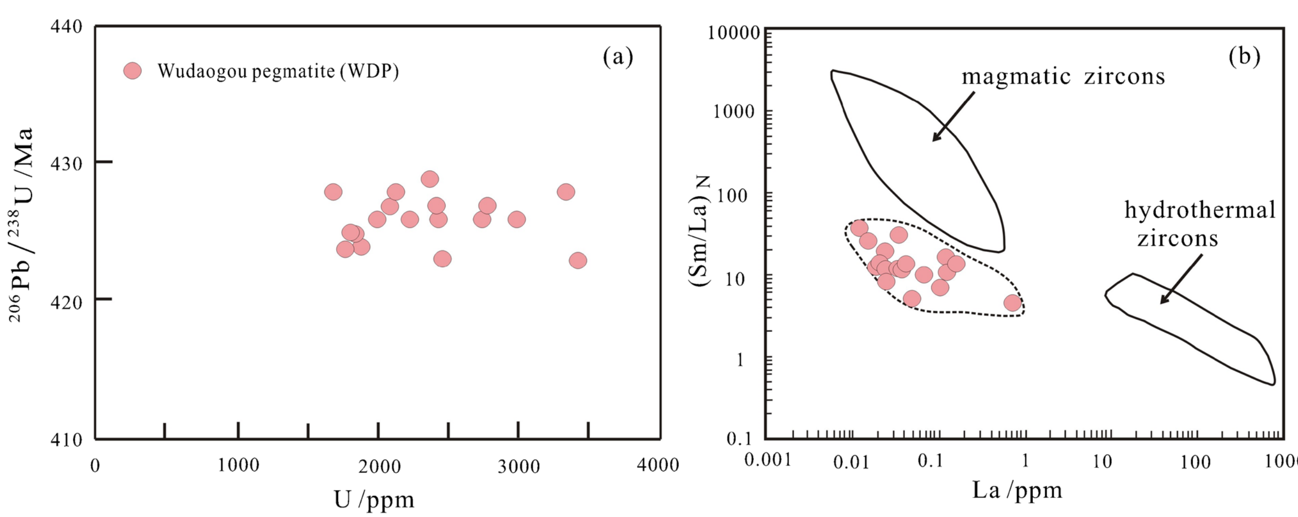

Fig. 9 Discrimination diagrams of **a** ^{206}Pb/^{238}U vs. U contents and **b** (Sm/La) $_N$ vs. La for zircons from Wudaogou pegmatites (after Hoskin (2005))

Combining our data with those from Chen et al. (2021b), the Wudaogou pluton as a whole has εHf(t) values of − 10.62 to 2.73, which suggest consistent εHf(t) values of granite and pegmatite.

In summary, we conclude that the Wudaogou pegmatite is closely related to the Wudaogou granitic pluton and formed as a result of the late magmatic evolution of the granitic body and the crystallization differentiation of apatite and allanite within the evolving magma.

Tectonic setting of the granitic and pegmatitic rocks

Early Paleozoic subduction-related intrusions have been discovered in the EKO, such as at Xiarihamu, Wulonggou, Nuomuhong (Huxiaoqin), Gelmo Zhiyu, Bairiqiete, Yikehalar, and Xiadawu (from west to east), with ages of 450–435 Ma (Chen et al. 2000; Liu, 2008; Liu et al. 2013; Jiang et al. 2015; Dong et al. 2018). Analysis of a high-Mg diorite–granodiorite complex from the central Kunlun suture zone, with an age of 432 Ma, suggests the cessation of subduction and initiation of collision, as well as slab break-off (Zhang et al. 2014), at around that time. Metamorphic rocks found in the Kunlun HP–UHP belt underwent peak metamorphism at 433–428 Ma in association with the final closure of the Proto-Tethys Ocean in the vicinity of the EKO at ca. 430 Ma (Meng et al. 2013; Qi et al. 2016; Du et al. 2017; Song et al. 2018).

Recently discovered intraplate volcanic rocks with ages of 428–425 Ma in the southern EKO (Chen et al. 2021a) suggest that an intraplate setting existed after ca. 430 Ma. Nearly contemporaneous A- and I-type granitic plutons (425–423 Ma) (Chen et al. 2021b; Norbu et al. 2021) provide further evidence for an extensional tectonic setting throughout the EKO since 428 Ma (Chen et al., 2021a,b). In addition, the Xiarihamu super-large copper–nickel sulfide deposit (Wang et al. 2014) and newly discovered Shitoukengde nickel–copper deposit (Zhou et al., 2015; Li, 2018; Li et al., 2018; Liu et al., 2018; Zhang et al. 2018; Jia et al., 2020; Norbu et al. 2020) that formed between ca. 425 and 420 Ma also confirmed the same result.

The Wudaogou granitic pluton and its pegmatite have ages of 428–425 Ma, coeval with granites and intraplate volcanic rocks in this area, which suggests that the Wudaogou rocks formed in a post-orogenic setting that was initiated when slab break-off triggered the abrupt cessation of collisional tectonism and rapid uplift (Chen et al. 2021b).

Conclusions

(1) Wudaogou pegmatite dikes have been discovered recently in the southern EKO. Zircon morphology and in situ trace element compositions suggest that zircons from the pegmatite formed in the transition stage between magmatic and hydrothermal zircons. The LA-ICP-MS zircon U–Pb age of the pegmatite is 425.8 ± 2.2 Ma, and that of the granodiorite is 427.7 ± 2.9 Ma, suggesting that the pegmatite was formed simultaneously with or slightly later than the granodiorite.

(2) Both the pegmatite and granodiorite samples have high silica contents, show a peraluminous nature, and belong to the medium-K and shoshonitic series. REE contents of the pegmatite are much lower than those of the granodiorite, most likely caused by crystal fractionation of accessory minerals, such as apatite, during magmatic evolution.

(3) Hf(t) values of the pegmatite range from − 3.89 to − 0.79 (mean = − 2.26) and those of the granodiorite range from − 7.53 to 2.73 (mean = − 2.48), suggesting a genetic relationship between the pegmatite and granodiorite that the pegmatite being a more highly differentiated product of the same magma from which the granodiorite was formed. These rocks formed in an extensional tectonic setting after the final closure of the Proto-Tethys Ocean in the EKO.

Supplementary Information The online version contains supplementary material available at https://doi.org/10.1007/s12517-022-10160-z.

Acknowledgements We thank Dr. H. Zhang for helping with the LA-ICP-MS U-Pb dating analysis and zircon Lu-Hf isotope analysis. We thank two anonymous reviewers for thoughtful reviews. Their constructive, stimulating, and insightful comments and suggestions helped to significantly improve this manuscript.

Funding This work was supported by the National Natural Science Foundation of China [Grant Numbers 41862011] and the CAS "Light of West China" Program.

Declarations

Conflict of interest The author declares no competing interests.

References

Andersen T (2002) Correction of common lead in U-Pb analyses that do not report ^{204}Pb. Chem Geol 192:59–79

Barnes EM, Weis D, Groat LA (2012) Significant Li isotope fractionation in geochemically evolved rare element-bearing pegmatites from the Little Nahanni Pegmatite Group, NWT, Canada. Lithos 132–133:21–36

Blichert TJ, Albarède F (1997) The Lu-Hf isotope geochemistry of chondrites and the evolution of the mantle-crust system. Earth Planet Sci Lett 148(1–2):243–258

Chen NS, Sun M, Zhang KX, Zhu YH (2000) Epidiorite ^{40}Ar-^{39}Ar and U-Pb geochronology of East Kunlun: the proof of remaining hornblende and Early Paleozoic magmatic belt of East Kunlun. Chin Sci Bull 45:2337–2342 (in Chinese with English abstract)

Chen GC, Pei XZ, Li RB, Li ZC, Pei L, Liu ZQ, Chen YX, Liu CJ, Gao JM, Wei FH (2013) Zircon U-Pb geochronology, geochemical characteristics and geological significance of Cocoe A'long quartz

diorites body from the Hongshuichuan area in East Kunlun. Acta Geol Sin 87:178–196
Chen B, Huang C, Zhao H (2020) Lithium and Nd isotopic constraints on the origin of Li-poor pegmatite with implications for Li mineralization. Chem Geol 551-119769. https://doi.org/10.1016/j.chemgeo.2020.119769
Chen J, Wang BZ, Li B, Yu FC (2021a) Silurian post-orogenic volcanic rocks of the South Kunlun Belt, NW China: links to the Proto- to Paleo-Tethyan tectonic transition. Int Geol Rev. https://doi.org/10.1080/00206814.2020.1867914
Chen J, Wang BZ, Yu FC, Han J, Li WF (2021b) Cessation of collisional tectonism and rapid uplift recorded by 430-420 Ma igneous rocks in the South Kunlun belt, northwest China. Int Geol Rev. https://doi.org/10.1080/00206814.2021.1995787
Chu NC, Taylor RN, Chavagnac V, Nesbitt RW, Boella RM, Milton JA, Germain CR, Bayon G, Burton K (2002) Hf isotope ratio analysis using multi-collector inductively coupled plasma mass spectrometry: an evaluation of isobaric interference corrections. J Anal at Spectrom 17:1567–1574
Dong YP, He DF, Sun SS, Liu XM, Zhou XH, Zhang FF, YangZ CB, Zhao GC, Li JH (2018) Subduction and accretionary tectonics of the East Kunlun orogen, western segment of the Central China Orogenic System. Earth Sci Rev 186:231–261
Du W, Jiang CY, Tang ZL, Xia MZ, Xia ZD, Ling JL, ZhouW WBY (2017) Discovery of the Dagele eclogite in East Kunlun, western China and its zircon SHRIMP U-Pb ages: new constrains on the central Kunlun suture zone. Acta Geologica Sinica (english Edition) 91(03):1153–1154
Fujimaki H (1986) Partition coefficients of Hf, Zr, and REE between zircon, apatite, and liquid. Contrib Miner Petrol 94(1):42–45
Griffin WL, Pearson NJ, Belousova E, Jackson SE, Van AE, O'Reilly SY, Shee SR (2000) The Hf isotope composition of cratonic mantle: LAM-MC-ICPMS analysis of zircon megacrysts in kimberlites. Geochim Cosmochim Acta 64:133–147
Hawkesworth CJ, Kemp AIS (2006) Using hafnium and oxygen isotopes in zircons to unravel the record of crustal evolution. Chem Geol 226(3–4):144–162
Henderson IHC, Ihlen PM (2004) Emplacement of polygeneration pegmatites in relation to Sveco-Norwegian contractional tectonics: examples from southern Norway. Precambrian Res 133:207–222
Hoskin PWO (2005) Trace-element composition of hydrothermal zircon and the alteration of Hadean zircon from the Jack Hills. Australia Geochimica Et Cosmochimica Acta 69(3):637–648
Hoskin PWO, Black LP (2000) Metamorphic zircon formation by solid-state recrystallization of protolith igneous zircon. J Metamorph Geol 18(4):423–439
Hoskin PWO, Ireland TR (2000) Rare earth element chemistry of zircon and its use as a provenance indicator. Geol 28(7):627–630
Hulsbosch N, Hertogen J, Dewaele S, Andre L, Muchez P (2014) Alkali metal and rare earth element evolution of rock-forming minerals from the Gatumba area pegmatites (Rwanda): quantitative assessment of crystal-melt fractionation in the regional zonation of pegmatite groups. Geochim Cosmochim Acta 132:349–374
Jia LH, Mao JW, Li BL, Zhang DY, Sun TT (2020) Geochronology and petrogenesis of the Late Silurian Shitoukengde mafic-ultramafic intrusion, NW China: implications for the tectonic setting and magmatic Ni-Cu mineralization in the East Kunlun Orogenic Belt. Int Geol Rev 60(4):1–22
Jiang CY, Ling JL, Zhou W, Du W, Wang ZX, Xia ZD, Xia MZ, Fan YZ, Song YF (2015) Petrogenesis of the Xiarihamu Ni-bearing layered mafic-ultramafic intrusion, East Kunlun: implications for its extensional island arc environment. Acta Petrologica Sinica 31:1117–1136
Jiang CF, Yang JS, Feng BG(1992) Opening-closing tectonics of the Kunlun Mts. Area. Beijing: Geol Publ House, 1–224(In Chinese with English abstract)
Kemp AIS, Hawkesworth CJ, Paterson BA, Kinny PD (2006) Episodic growth of the Gondwana supercontinent from hafnium and oxygen isotopes in zircons: Natur,m 439:580–583.
Li JK, Chou IM (2016) An occurrence of metastable cristobalite in spodumene-hosted crystal-rich inclusions from Jiajika pegmatite deposit. China J Geochem Explor 171:29–36
Li RS, Ji WH, Yang YC, Yu PS, Zhao ZM, Chen SJ, Meng Y, Pan XP, Shi BD, Zhang WJ, Li X, Luo CY (2008) Kunlun Mountains and geology of adjacent areas. Geol Publ House, Beijing:1–400 (in Chinese with English abstract)
Li L, Sun FY, Li BL, Li SJ, Chen GJ, Wang W, Yan JM, Zhao TF, Dong J, Zhang DX (2018a) Geochronology, geochemistry and Sr-Nd-Pb-Hf isotopes of No. I complex from the Shitoukengde Ni-Cu sulfide deposit in the Eastern Kunlun Orogen, Western China: implications for the magmatic source, geodynamic setting and genesis: Acta Geologica Sinica (English Edition) 92(1):106–126.
Li L (2018) Features of the mafic-ultramafic rocks in the Periphery of Qaidam Block, Qinghai Province and their metallogenesis. Jilin University (Changchun), Ph.D. thesis: 80–227 (In Chinese with English abstract)
Liu YJ, Genser J, Neubauer F, Jin W, Ge XH, Handler R, Takasu A (2005) ^{40}Ar/^{39}Ar mineral ages from basement rocks in the Eastern Kunlun Mountains, NW China, and their tectonic implications. Tectonophysics 398:199–224
Liu YS, Hu ZC, Gao S, Günther D, Xu J, Gao CG, Chen HH (2008) In situ analysis of major and trace elements of anhydrous minerals by LA-ICP-MS without applying an internal standard. Chem Geol 257(1–2):34–43
Liu B, Ma CQ, Jiang HA, Guo P, Zhang JY, Xiong FH (2013) Early Paleozoic tectonic transition from ocean subduction to collisional orogeny in the Eastern Kunlun region: Evidence from Huxiaoqin mafic rocks. Acta Petrologica Sinica 29:2093–2106
Liu YG, Li WY, Jia QZ, Zhang ZW, Wang ZA, Zhang ZB, Zhang JW, Qian B (2018) The dynamic sulfide saturation process and a possible slab break-off model for the giant Xiarihamu magmatic nickel ore deposit in the East Kunlun orogenic belt, Northern Qinghai-Tibet Plateau. China Econ Geol 113(6):1383–1417
London D (2018) Ore-forming processes within granitic pegmatites. Ore Geol Rev 101:349–383
Ludwig KR (2003) Isoplot/Ex version 3.00: a geochronological toolkit for Microsoft Excel: Berkeley Geochronology Center, Berkeley, CA.
Mahood G, Hildreth W (1983) Large partition coefficients for trace elements in high-silica rhyolites. Geochim Cosmochim Acta 47(1):11–30
Meng FC, Zhang JX, Cui MH (2013) Discovery of Early Paleozoic eclogite from the East Kunlun, Western China and its tectonic significance. Gondwana Res 23:825–836
Middlemost EAK (1985) Magmas and magmatic rocks. Longman, London, pp 1–266
Norbu N, Li J, Liu Y, Jia Q, Kong H (2020) Tectonomagmatic setting and Cu-Ni mineralization potential of the Gayahedonggou Complex, Northern Qinghai-Tibetan Plateau. China Minerals 10(11):950
Norbu N, Liu Y, Li J, Jia Q, Wang W, Song X, Li Y, Kong H, Gao Y, Guo X (2021) The Silurian-Devonian granitoids in the East Kunlun orogenic belt, northern Qinghai-Tibetan plateau, China: origin and tectonic implications. Geosci J 25(6):763–786
Peccerillo R, Taylor SR (1976) Geochemistry of Eocene calc-alkaline volcanic rocks from the Kastamonu area. Northern Turkey Contrib Mineral Petrol 58:63–81

Qi X, Yang J, Fan X (2016) Age, geochemical characteristics and tectonic significance of Changshishan ophiolite in central East Kunlun tectonic melange belt along the east section of East Kunlun Mountains. Geol China 43:797–816 (in Chinese with English abstract)

Song SG, Bi HZ, Qi SS, Yang LM, Su L, Li WF (2018) HP-UHP metamorphic belt in the East Kunlun Orogen: final closure of the Proto-Tethys Ocean and formation of the Pan-North-China continent. J Petrol 59(11):2043–2060

Stewart DB (1978) Petrogenesis of lithium-rich pegmatites. Am Mineral 63:970–980

Sun SS, McDonough WF (1989) Chemical and Isotopic Systematics of Oceanic Basalts: Implications for Mantle Composition and Processes: Geol Soc London Spec Publ 42:313–345

Sun H, Gao YJ, Xiao YL, Gu HO, Casey JF (2016) Lithium isotope fractionation during incongruent melting: constraints from post-collisional leucogranite and residual enclaves from Bengbu Uplift. China Chem Geol 439:71–82

Thomas R, Webster JD, Heinrich W (2000) Melt inclusions in pegmatite quartz: complete miscibility between silicate melts and hydrous fluids at low pressure. Contrib Mineral Petrol 139:394–401

Wang XX, Hu NG, Wang T, Sun YG, Ju SC, Lu XX, Li S, Qi QJ (2012) Late Ordovician Wanbaogou granitoid pluton from the southern margin of the Qaidam basin: zircon SHRIMP U-Pb age, Hf isotope and geochemistry. Acta Petrologica Sinica 28:2950–2962

Wang G, Sun F, Li B (2014) Zircon U-Pb geochronology and geochemistry of the mafic-ultramafic intrusion in Xiarihamu Cu-Ni deposit from East Kunlun, with implications for geodynamic setting. Earth Sci Front 21:381–401 (in Chinese with English abstract)

Wang GC, Wei QR, Jia CX, Zhang KX, Li DW, Zhu YH, Xiang SY (2007) Some ideas of Precambrian geology in the East Kunlun, China: geological Bulletin of China 26:929–937.

Wiedenbeck M, Allé P, Corfu F, Griffin WL, Meier M, Oberli F, von Quadt A, Roddick JC, Spiegel W (1995) Three natural zircon standards for U-Th-Pb, Lu-Hf, trace element and REE analyses. Geost and Newsl 19:1–23

Wilson M (1989) Igneous petrogenesis: London, Chapman &Hall 1–366.

Wu FY, Yang YH, Xie LW, Yang JH, Xu P (2006) Hf isotopic compositions of the standard zircons and baddeleyites used in U-Pb geochronology. Chem Geol 234:105–126

Wu FY, Li XH, Zheng YF, Gao S (2007) Lu-Hf isotopic systematics and their applications in petrology. Acta Petrologica Sinica 23(2):185–220 (in Chinese with English abstract)

Wu C, Zuza AV, Chen X, Ding L, Levy DA, Liu C, Liu W, Jiang T, Stockli DF (2019) Tectonics of the Eastern Kunlun Range: Cenozoic reactivation of a Paleozoic-Early Mesozoic orogen. Tectonics 38:1609–1650

Xu X, Song SG, Su L (2016) Formation age and tectonic significance of the Wanbaogou basalts in the middle East Kunlun orogenic belt. Acta Petraologica Et Mineralogica 36(6):965–980

Yurimoto H, Duke EF, Papike JJ, Shearer CK (1990) Are discontinuous chondrite-normalized REE patterns in pegmatitic granite systems the results of monazite fractionation. Geochim Cosmochim Acta 54(7):2141–2145

Zhang JY, Ma CQ, Xiong FH, Bin L, Li JW, Pan YM (2014) Early Paleozoic high-Mg diorite-granodiorite in the eastern Kunlun Orogen, western China: response to continental collision and slab break-off. Lithos 210–211:129–146

Zhang ZW, Wang YL, Qian B, Liu YG, Zhang DY, Lv PR, Dong J (2018) Metallogeny and ectonomagmatic setting of Ni-Cu magmatic sulfide mineralization, number I Shitoukengde mafic-ultramafic complex, East Kunlun Orogenic Belt, NW China. Ore Geol Rev 96:236–246

Zhou W, Du W, Wang ZX (2015) Geochronology and its significance of the mafic-ultramafic complex in Shitoukengde Cu-Ni mineral occurrence, Eastern Kunlun. J of Jilin Univ (Earth Science Edition) 45(sup.1):1–2(In Chinese with English abstract)